The visible spectrum of highly charged ions: A window to fundamental physics[1]

J.R. Crespo López-Urrutia

Abstract: The observation of forbidden transitions in the visible range was the first experimental sign of the existence of highly charged ions in nature. Such lines can nowadays be excited in electron beam ion traps with excellent control of the ionic charge state, allowing their identification and precise determination of wavelengths and transition probabilities. The accuracy achieved in such experiments has been central to the study of nuclear size effects and quantum electrodynamic contributions, which are drastically magnified in highly charged ions, thus enabling the study of the underlying fundamental interactions in few-electron systems. At the same time, forbidden lines can be used to probe conditions in high temperature plasmas present in both astrophysical and laboratory environments.

PACS Nos.: 31.30.Jv, 32.10.Fn, 32.30.Jc, 96.60.Tf, 97.10.Ex, 32.60.+i, 32.70.Cs, 12.20.Fv, 42.50.Xa

Résumé : L'observation de transitions interdites dans le visible a été le premier signe expérimental de l'existence d'ions hautement chargés dans la nature. Aujourd'hui, de telles lignes peuvent être excitées dans des pièges ioniques à faisceau d'électrons avec un excellent contrôle de la charge ionique, permettant leur identification et la détermination précise de leurs longueurs d'onde et de leurs probabilités de transition. La précision atteinte joue un rôle central dans l'étude des effets dus à la dimension du noyau et d'autres effets QED fondamentaux, qui sont significativement amplifiés dans les ions très chargés, permettant ainsi l'étude sous-jacente fondamentale des interactions dans les systèmes à peu d'électrons. Simultanément, les lignes interdites peuvent être utilisées pour sonder les conditions qui prévalent dans les plasmas de haute température présents en astrophysique et dans le laboratoire.

[Traduit par la Rédaction]

1. Introduction

The most natural energy scale for highly charged ions (HCI) is obviously related to the energy differences between levels of different principal quantum number n. With those differences rapidly scaling up proportionally to the square of the atomic number Z, the X-ray region becomes the spectral range of choice for spectroscopic research on HCI. Despite the large body of work assembled over the last decades in this field, experimental difficulties related to the low efficiency of crystal spectrometers and their complicated calibration still limit the accuracy of the data to the level of a few parts per million in the best of cases. The atmospheric absorption of the X-rays from other celestial bodies precluded until very recently detailed astronomical observations in this range. However, relativistic effects growing with Z^4 split the ground configurations of HCI far enough to give rise to energy differences amenable to optical spectroscopy. The situation in general is such that the wave function symmetry properties forbid electric dipole (E1) transitions in these cases. Nonetheless, magnetic-dipole (M1) type electronic transitions are not excluded, and even though the corresponding transition probabilities, as a result of the magnitude of the M1 transition operator, are intrinsically nearly a million times weaker than their E1-allowed counterparts, favorable excitation mechanisms in tenuous plasmas still lead to line intensities high enough for detection. It was in the last third of the XIXth century that spectral recordings of the solar corona registered during the 1869 total solar eclipse showed the presence of strong lines due to the then unknown HCI. On 7 August 1869, Harkness and Young [1] discovered an emission line in the green part of the spectrum. Young (1879) identified the line as the Fe Line No. 1474 on Kirchoff's scale. It was surprising that only a single intense line out of the hundreds of known iron lines should be observed in the coronal spectrum and that it should appear at such great heights above the solar surface. A controversy ensued due to the impossibility of assigning this as well as some other detected lines to any of the then known elements, which was fed by the fact that the obvious temperature of the solar surface as seen from Earth was different by orders of magnitude. The explanation for the unidentifiable lines remained elusive, and it took more than 60 years to arrive at an acceptable interpretation of their origin, namely, the high temperatures prevalent in the corona.

Grotrian analyzed the spectra obtained in Sumatra during the 1929 solar eclipse [2]. Figure 1 shows an example of that work, the intensity profile of the mysterious "red line" at 6374 Å as function of the angular separation from the surface of the Sun.

After a pioneering semi-empirical analysis of the term differences and extrapolation of those to high-charge states [3] in the year 1939, it dawned on him that

> ... in the outer zones of the solar atmosphere con-

Received 22 May 2007. Accepted 25 June 2007. Published on the NRC Research Press Web site at http://cjp.nrc.ca/ on 26 January 2008.

J.R. Crespo López-Urrutia. Max Planck Institute for Nuclear Physics, D-69117 Heidelberg, Germany (e-mail: crespojr@mpi-hd.mpg.de).

[1] Paper given at the Workshop on Twenty Years of Spectroscopy with EBIT held in Berkeley, California, 13–15 November 2006.

 doi: 10.1139/P07-115

Fig. 1. Two intensity profiles of the then still unidentified "red line" [2] recorded during the 1929 total solar eclipse in Sumatra by a Dutch–German expedition. The abscissa refers to the angular separation from the edge of the Sun; one arc minute (′) corresponds to a height of roughly 44 000 km above the Sun. From ref. 2, published with permission of Springer Verlag.

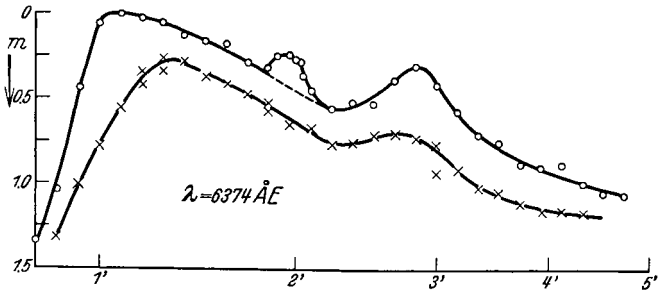

> ditions for the excitation of spectral lines exist exceeding by far what would be expected under thermal equilibrium, it appears that discussing the question of the possibility of the coronal lines being interpreted as forbidden transitions from highly ionized atoms is not entirely absurd. …The agreement is thereafter as good as one can expect in view of the accuracy by which the difference of the terms has been determined. [3]

Since then, his scientific weight, in combination with Edlén's further studies, gained, with time, acceptance of the audacious hypothesis in the astrophysical community. In an extremely thorough work presented in the year 1942, Edlén [4] compared the theoretical wavelengths of the postulated highly charged ions systematically with the observed coronal line data for various isoelectronic sequences of Ar, Ca, Fe, Ni, and analyzed the possible excitation mechanisms for these transitions by electronic collisions and photoexcitation, as well as by the quenching process, which he correctly derived. By these means, 23 lines were identified definitively. The spectral line width of these lines, which had been determined by Lyot [5] was correctly interpreted as arising from the Doppler-broadening associated with temperatures of several hundred thousand degrees. After assembling all this evidence, Edlén could finally conclude "The final result represents a practically complete explanation of the observed coronal lines." and proclaim rightly that "At the same time, pathbreaking conclusions on the ionization and excitation conditions in the corona are inferred." He pointed to a 1941 theoretical paper of Alfvén [6] that had proposed a heating mechanism and also dealt with the conditions in the solar corona for possible explanation of the hitherto unexpected and now experimentally confirmed high temperatures. The presence of the Fe XIV line at 530.3 nm, the Fe X line at 637.4 nm, and three other coronal lines in the spectrum of the nova-like star, RS Ophiuchi, showed that such conditions were not uncommon in the Universe.

The advantages of optical spectroscopic methods for diagnostic purposes are manifold. Light can be transmitted through glass fibers, images can be taken with high spatial and spectral resolution, the large solid angle subtended by standard optics makes intensity problems less acute than in other spectral regions, and a great variety of imaging and non-imaging detection systems with quantum efficiencies in some cases higher than 90% are available. The optical telescope, unfettered by atmospheric absorption and upgraded with adaptive optics, is still the instrument of choice for deep astronomical observations, and is now able to resolve in interferometric configurations minute spectral shifts induced in stellar emission lines by the gravitational pull of the numerous planets hitherto hidden to man. As an example of an application closer to daily life, chemical analysis also relies largely on atomic emission spectroscopy. The now universally widespread charge-coupled device (CCD) is finding manifold uses in spectroscopic techniques, which have now become inexpensive and reliable for general applications. Optical fiber networks have become the equivalent circulatory system of modern societies, due to the amazing bandwidth that they carry, all based on spectral control of the transmitted photons. In short, photonics, the new and suggestive name of this large plethora of optical and spectroscopic techniques, is gaining ground in all possible aspects of life. At the same time, optical spectroscopy has still retained its momentum in fundamental research. The development of laser spectroscopy in the last decades represents a formidable boost for atomic and plasma physics research, and this technique has finally established itself as the most accurate method currently available to physicists. Indeed, laser spectroscopy is now capable of superseding the existing atomic clock standards and of such experimental feats as testing the time variation of the fine structure constant α, one of the most accurately known constants, over the lifetime of our Universe (see work by Hänsch's group [7]). In this context, it is noteworthy to mention that first indications for a possible shift of the order of $\delta\alpha/\delta t \approx 10^{-15}$ per year had been found in the statistical analysis of lines with different $\delta\lambda/\delta\alpha$ (λ being the wavelength) dependence observed in the spectra of quasars at high redshifts [8], but that further astronomical observations with somewhat improved accuracy [9] have more recently yielded a time variation consistent with zero.

Forbidden lines are characteristic for unfilled subshell configurations of HCI. The long lifetimes of the upper levels in these transitions lead to a strong dependence of their intensity on the plasma density. Collisions with electrons and other particles depopulate the excited state, and, therefore, these type of lines only appear in tenuous plasmas. This property makes the lines suitable for density diagnostics. As mentioned above, natural radiation sources exist for them. Lines arising from transitions within $2s^l 2p^m$, $2s^2 2p^3 3d$ configurations or similar electronic structures have been detected in astrophysical sources (see, for example, an early compilation by Swings [10], a newer survey by Wagner and House [11], or a recent concrete example in ref. 12). Some observations in high-temperature, fusion-related plasmas, are recompiled in refs. 13–15. Spectral data have also been obtained using electron cyclotron ion sources and ions extracted from them [16]. In fusion plasmas and most ion sources, however, line positions tend to suffer from systematic shifts due to contributions of satellite (i.e., spectator) electrons due to multiple excitation or following electron capture.

For these reasons, interesting applications for those forbidden lines emitted by HCI were proposed early. Soon after HCI were

produced for the first time in the laboratory by different means, these transitions could be observed in a more or less controlled way. Applications to plasma diagnostics were quickly found. The electronic structure of HCI constitutes by itself an interesting object of study. In this regard, their relativistic origin and their sensitivity to contributions from quantum electrodynamics (QED) and nuclear-size effects soon became obvious, and stimulated new experiments aimed at the investigation of such effects.

2. The electron beam ion trap application to visible spectroscopy

The electron beam ion trap (EBIT) first appeared in the field of HCI physics in the year 1986, at the Lawrence Livermore National Laboratory (LLNL). The essential contributions for its development came from Levine and Marrs [17, 18]. Since then, the study of ions in the highest possible charge states at rest in a small confined volume became feasible. Easy control of the ionization stage and of resonant excitation channels could be achieved by tuning the electron energy of the device to the respective ionization thresholds or resonances. The extremely high vacuum level (10^{-12} mbar) reached within the trap made it a natural experimental simulation chamber for very low-density plasmas with the electronic level population dominated by electronic collisions, close to the conditions of coronal equilibrium in the Sun. Due to these features, the EBIT would quickly evolved into a workhorse for the spectroscopy of HCI [19]. At first, studies in the X-ray region were at the center of attention, since new opportunities for the study of processes like dielectronic recombination at high collision energies, among many others, became possible with it. But interest in the visible spectrum of EBIT-trapped HCI soon arose.

The first experiment with an EBIT in the visible range was motivated by an idea put forward in the year 1991 in a paper by Feldman et al. [20]. It was about an exciting perspective, namely, that an ion in a charge state as high as U^{70+} (U LXXI in spectroscopic notation) could emit light in the near ultraviolet range at 320 nm, or even in the visible. The Ti-like ($Z = 22$) configuration $3d^4$ of that type of ion has electronic levels very close to the ground state, capable of generating such lines. Still more interesting was the ability to show that the mutual compensation of different binding energy contributions in that isoelectronic series makes the wavelength of some of these M1 lines, and in particular those of the $3d^4\,{}^5D_3 \rightarrow {}^5D_2$ transition, rather insensitive to variations of Z. This was a unique property, since nearly all other then known electronic transitions scale their energies with high powers of Z. In this case, a comparatively narrow region of the spectrum could be used to detect and investigate HCI from elements across the upper half of the Periodic Table. Predictions from Nd XXXIV on were quickly tabulated.

Morgan et al. succeeded in 1994 [21] in observing visible radiation originating from the $3d^4\,{}^5D_2 \rightarrow {}^5D_3$ transition in Ba^{34+} trapped at the NIST EBIT [22]. Earlier attempts to observe the Zeeman splitting of the line by using a Fabry–Perot interferometer had failed [23], due to the high ion temperatures between 500 and 1000 eV prevalent in the trap configuration chosen for that

Fig. 2. The Ba^{34+} $3d^4\,{}^5D_3 \rightarrow {}^5D_2$ optical transition as registered by Morgan et al. [21] at the NIST EBIT was the first observed in such a device. This figure is reproduced with the permission of the American Physical Society. ©APS Journals.

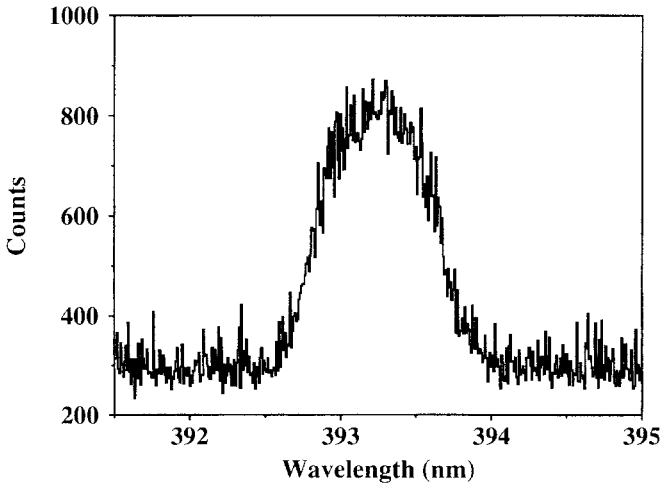

measurement, which caused a large Doppler width of the lines. Morgan also investigated the analogous transition for Xe^{32+}, and found new lines in the neighboring isoelectronic V-like sequence. The charge states of the ions responsible for the line emission were inferred from the electron beam energy threshold at which the lines appeared. In fact, in good agreement with the expectations, a sharp intensity rise was observed at energies around 2 keV. The maximum was reached within ≈100 eV from that threshold, and intensity decreased half as steeply at higher energies. This was attributed to the further ionization of the Ba ion inventory to higher charge states. The experiments at NIST were initially performed by imaging the trap region onto the entrance slit of a 0.25 m focal length, $f = 3:5$ Ebert-grating monochromator equipped with a photomultiplier tube and scanning it across the predicted spectral range. For calibration, light from low-pressure discharge lamps was projected onto the entrance slit through the EBIT using a port opposite to the spectral instrument. Lines from low-charge Kr and Ar ions also trapped in the EBIT were used as well. The lines of interest displayed a FWHM of 0.8 nm, sufficient to determine their central wavelengths with an estimated uncertainty of ±0.2 nm. The result for Ba^{34+} was found to be 393.2(2) nm (see Fig. 2), in significant disagreement with the value of 377.8 nm predicted in ref. 20. Later, more sophisticated multiconfiguration Dirac–Fock calculations still showed a 4% deviation from the experimental data, which were already accurate at the level of 0.05%. Better agreement was found with calculations obtained with the relativistic multiconfiguration Hartree–Fock method implemented in the Cowan code [24] by a semiempirical scaling of the F_k Slater integrals to 93% of their initial theoretical values to adjust the wave functions to agree with the Ba results. This scaling, however, was of little use when extrapolated to other analogous transitions, with predictions disagreeing with the data by up to 5 nm. Nonetheless, the Cowan code generated the best overall agreement at that time and was reasonably successful in helping to identify lines in other spectra.

In a later experiment [25] transitions in the Ti-like sequence from Nd^{38+} and Gd^{42+} were investigated to verify the expected wavelength scaling behavior. The wavelength data resulting from those measurements had an overall uncertainty of less than ±0.2 nm, and was useful, in combination with the earlier Xe and Ba data, to adjust the values of F_k Slater integrals within the Cowan code [24] to 0.922, 0.930, 0.946, 0.962 for Xe, Ba, Nd, and Gd, respectively. This semiempirical scaling was extrapolated to higher Z by a linear variation of the scale factor $0.922 + 0.004 \times (Z - 54)$ to obtain better wavelength estimates for the Ti-like ions up to Os ($Z = 76$), for which the scaling factor was already equal to 1.0. A weak peak at 314.4 nm found at the same electron beam energy was tentatively identified as due to the $3d^4\ {}^5D_4 \rightarrow {}^5D_3$ transition in the ground state configuration of Gd^{42+}. Another result given in ref. 25 was an enhancement of the Ti-like population due to resonant dielectronic recombination (DR) from the Sc-like Gd^{43+} at around 3.8 keV beam energy, leading to intensified emission of the forbidden visible line.

Further experiments by Serpa et al. [26] yielded more data on the spectra of highly ionized Kr, in which they found new lines. The possible effects of the Zeeman and Stark effects on the wavelength were discussed in that work. Although the electrostatic field on the edge of the electron beam in an EBIT reaches high values of 10^8 V/cm, no noticeable Stark shift or broadening were found, as could have been expected from the low polarizability of the deeply bound optical electron in HCI. The Zeeman splitting, being symmetric due to the small ratio between the magnetic field orientation energy and the large fine structure splitting of the levels, which is the very reason for the appearance of forbidden lines, does not induce a measurable shift of the central wavelength, even at the high magnetic field values found in EBITs.

It is important to mention here that by applying both the standard (i.e., by means of the electron beam space charge potential) and the magnetic trapping mode of an EBIT [27], lifetimes of metastable levels in the range $\tau = 10^{-7}...10^{-1}$ s can be measured very precisely. Serpa applied this method to the forbidden transitions of Kr [28], and Ar and Kr [29]. Information on those experiments can be found in the review of Gillaspy [30]. More results obtained with this technique, which in most cases achieve a relative accuracy $\delta\tau/\tau$ around 2%, but in some cases approach a value of 0.1% (in which case QED contributions to the transition probability become apparent), are reported by Träbert et al. [31–33], Beiersdorfer et al. [34], Lapierre et al. [35, 36], and Brenner et al. [37]. An example of the application of this technique is illustrated on Fig. 3.

Other EBIT groups pursued further studies on the Ti-like isoelectronic sequence. After initial results obtained at the Tokyo EBIT and reported by Currell in 1999 [38, 39], more systematic work on the wavelengths of the $3d^4\ {}^5D_3 \rightarrow {}^5D_2$ transition in Ti-like ions was carried out by Watanabe et al. (see, for example, refs. 40 and 41 and references therein). The data collected in the range $Z = 51$ to 83 had a typical relative accuracy of $\delta\lambda/\lambda \approx \pm 100$ ppm. Still, predictions departed from experiment by more than five times that figure. The calculations suffered from the complexities of the interelectronic coupling in open subshells, and from the lack of adequate ab initio predictions

Fig. 3. Lifetime measurements of long-lived forbidden transitions are performed in an EBIT without electronic quenching effects using the so-called magnetic trapping mode [27]. The electron beam is cyclically turned on and off. During the off periods, the electronic relaxation of the metastable levels by photon emission is monitored with time resolution using, in the case of visible lines, a photomultiplier tube.

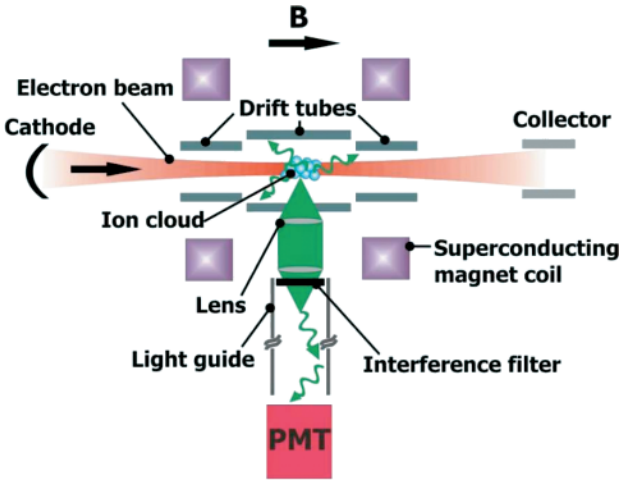

of the already sizable QED contributions to the binding energy. The Tokyo EBIT group also developed a diagnostic tool for the properties of the electron beam in the EBIT by analyzing the Thompson scattering of a laser (532 nm wavelength) injected into the EBIT [42]. The results (values of the electron beam radius around 30 μm) agreed well with the predictions of the Herrmann model [43]. At the LLNL EBIT, Träbert [31] detected a transition in Si-like Mo^{28+} at 284.0(2) nm, confirming an earlier identification from tokamak plasmas. In the same work, Träbert also reported the $3d^4\ {}^5D_3 \rightarrow {}^5D_2$ transition in Ti-like Au^{57+} at 353.2(2) nm.

Porto studied the spatial distribution of the trapped ions at the NIST EBIT [44], and also obtained translational temperature information. Porto continued investigating the Ti-like sequence, observing the corresponding ytterbium, tungsten, and bismuth ions [45]. Working at the same machine, Tákacs recently reported an identification of a Xe^{9+} transition at 598.30(13) nm [46]. This transition has been unambiguously identified as arising from the Xe^{9+} by Biedermann at 598.04(3) nm, [47] who also found a Xe^{31+} line at 598.21(3) nm, confirming the earlier observation of that feature at electron beam energies higher than 1900 eV by Crespo et al. at 598.4(1.0) nm in their survey work [48–50].

A tenfold increase in accuracy achieving values of $\delta\lambda/\lambda$ below 10 ppm was first achieved at the Oxford EBIT by Silver's group [51], by Bieber [52], and by Bieber et al. [53] in 1997, with precise measurements of the $3d^4\ {}^5D_3 \rightarrow {}^5D_2$ line in Sn^{28+} at 498.189(6) nm, in Ag^{25+} at 631.481(4) nm [54], and also with studies of the Ar^{13+} and Ar^{14+} coronal lines.

In a different approach following an idea reported by Margolis in 1996 [55], Back et al. [56] used a laser to determine the Lamb shift in H-like Si^{12+} ions by depopulating the metastable $2s_{1/2}$ level. The laser transferred the population into the $2p_{3/2}$

Fig. 4. Setup for the acquisition of spatially resolved visible spectra at the LLNL SuperEBIT. In this slitless setup, an image of the trap region is projected through a prism spectrograph onto a cryogenically cooled charge-coupled device. This technique yields wide spectral coverage, good light collection efficiency, and a very low-noise figure.

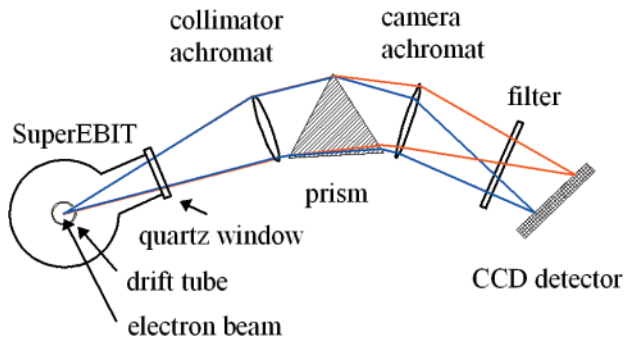

Fig. 5. Series of spectra emitted by Ba ions trapped at the LLNL EBIT-II as function of the electron beam energy. Lines appear and vanish as higher ionization stages (indicated on the left axis) are produced, while lower stages are depleted (shown on the right-hand side), with rising electron beam energy.

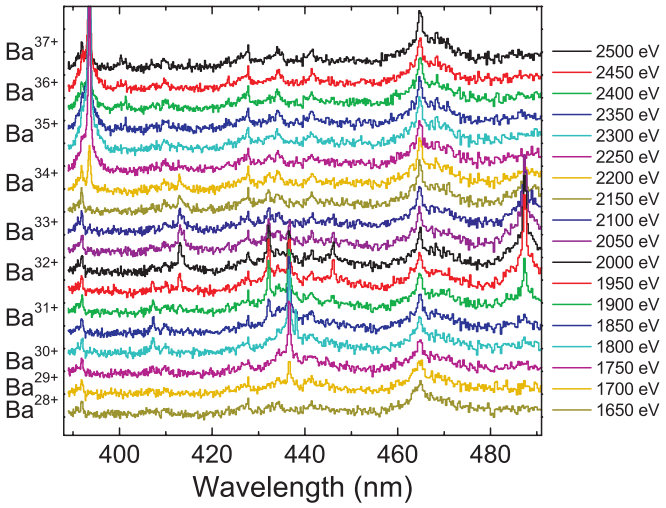

level, and the X-ray fluorescence resulting from the decay of that level to the ground state was detected. The large natural width of the short-lived $2p_{3/2}$ level limited the accuracy of the Lamb-shift determination by broadening the resonance curve obtained by tuning the laser. For the first time, attempts were also made to apply laser spectroscopy to the investigation of the $1s^2\,2s\,2p\,{}^3\mathrm{P}_2 \rightarrow {}^3\mathrm{P}_1$ transition in Be-like Ar^{13+} [57].

3. Charge state identification and spatial distributions of trapped HCI

Work on optical spectroscopy at the LLNL SuperEBIT, a device capable of producing H-like and even bare ions up to U^{92+}, had initially proceeded with an imaging prism spectrograph, as shown in Fig. 4. The use of a cryogenically cooled CCD camera with a very low-noise figure of typically less than 0.01 e^- per pixel per hour allowed the investigation of very weak visible transitions practically without any other background than that caused by cosmic radiation on the CCD detector during the hour-long exposure times. The signal generated by such cosmic events, however, could be eliminated by its topology (single, isolated spots on the camera) and by pulse height discrimination. Each pixel on the CCD acted as an individual energy-sensitive detector, with optical photons typically generating only one photoelectron, and X-rays and energetic particles producing hundreds and thousands of electrons per pixel. An optical line on the focal plane of the spectrograph illuminates an area of several hundred pixels in length and a few in width, in total several thousand pixels. At the background level attainable after discrimination, photon fluxes on the line down to the order of a few tens of photons per hour could be reliably detected, and resulted in useful spectra after accordingly repeated acquisitions and long integration times.

Fig. 6. A spatially resolved spectrum obtained at the LLNL EBIT. The spectrum stretches horizontally from 384 to 481 nm (nonlinear scale). A 4 mm broad Xe atomic beam crosses the electron beam (diameter 70 μm) at the trap center region. The short lines are produced by Xe atoms and low-charge-state ions excited there, which promptly decay by E1-allowed transitions ($\tau \approx$ ns). Ions trapped by the space-charge potential of the electron beam are then further ionized and fill the whole trap length (vertically 20 mm, given by the drift tube separation). Metastable levels populated in $Xe^{18+,31+,32+}$ ions by sequential electron impact excitation decay very slowly ($\tau \approx$ ms) by forbidden transitions taking place along the whole trap (long lines), and display a wider radial distribution (reflected in the horizontal line width) with diameters up to 1 mm because of their higher temperature.

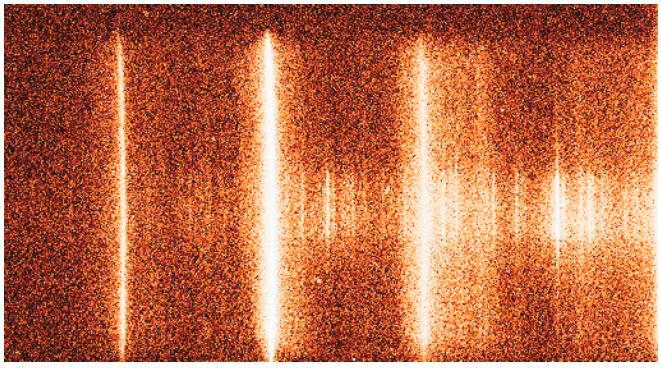

The imaging spectrograph at the LLNL EBIT has became a very appropriate tool for studying the spatial distributions of the light-emitting species in the EBIT since 1995 [48], and its high efficiency allowed systematic studies of the electron beam energy dependence of the spectra. The wide spectral range covered in a single exposure was very advantageous in this regard. Exposure times of tens of minutes were sufficient in most cases to record good-quality spectra at a given energy. Spectra of Kr, Xe, and Ba in different charge states are collected in ref. 50. An example for Ba^{28+}...Ba^{37+} is depicted in Fig. 5. No entrance slit was used in this setup, in which the spectrally

Fig. 7. Projection of a spatially resolved spectrum (like the one depicted in Fig. 6) containing the strong Ar^{13+} $1s^2\,2s^2\,2p\,^2P_{3/2} \rightarrow {}^2P_{1/2}$ transition at 441.256 nm. The Ar atoms deexcite promptly within the electron beam through an electric dipole transition. The apparent width of 150 μm FWHM for the Ar lines includes broadening due to the apparatus profile. The Ar^{13+} ions show a much wider line (1000 μm FWHM), since under the chosen trapping conditions their higher temperature induces much larger excursions from the trap center before the metastable upper level involved in the transition can decay.

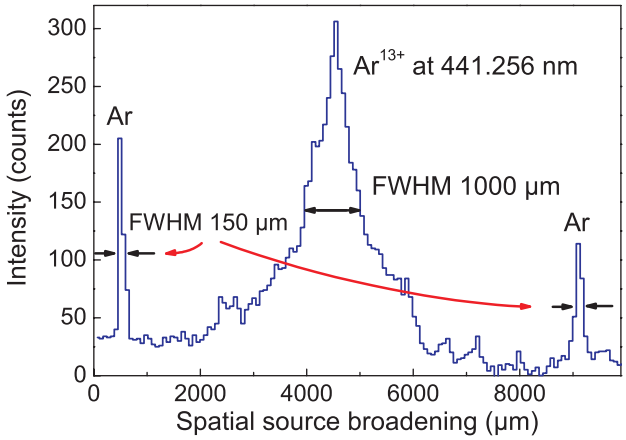

resolved image of the narrow ion cloud was projected onto the focal plane of the spectrograph. It was, therefore, possible to observe the differences in spatial distribution for ions and neutrals injected into the trap, as shown in Fig. 6 for Xe ions.

The projected spectra display clear differences for the distribution of neutrals and HCI, exemplified in Fig. 7 for the case of Ar. The ions displayed much wider line profiles than the neutrals crossing the electron beam. This phenomenon is caused by the lifetime of the excited states, by the spatial distribution of the emitting species, and by temperature effects. The neutrals, injected at room temperature ($kT \approx 25$ meV), and the singly charged ions produced initially move at low velocity through the narrow electron beam. Their excited levels decay promptly ($\tau \approx$ ns) by E1-allowed transitions while they are still within the electron beam diameter. Therefore, the light emitted by them reflects the overlap between the spatial distribution of those species and the electron beam. In contrast, the trapped HCI are heated to high translational temperatures on the order of $kT \approx 1$ keV, and oscillate accordingly with much larger velocity within the trap region, performing larger radial excursions from the electron beam before decaying. The combined effect of cyclotron motion and trapping by the electron beam space charge as well as by the applied axial potential determines their overall spatial spread. The longer lifetimes of the upper states of the M1 transitions decouples the spatial distribution of the optical decay from the geometry of the excitation region, i.e., the electron beam pathway, and makes the light intensity map a good monitor for the ion spatial distribution.

Chen et al. carried out systematic surveys of the optical spectrum of Kr HCI [58], where they identified many new lines mainly with the purpose of selecting transitions appropriate for the plasma diagnostics in tokamaks. The LLNL group carried

Fig. 8. Spectrum of the hyperfine transition $1s\,^1S_{1/2}$, $F = 1 \rightarrow 0$ in the ground state of the $^{207}Pb^{81+}$ ion obtained by Seelig et al. [65] at the GSI ESR storage ring by collinear laser spectroscopy. Note that the ion velocity uncertainty induces an error bar larger than the observed line width. Reproduced with permission from the American Physical Society. ©APS Journals.

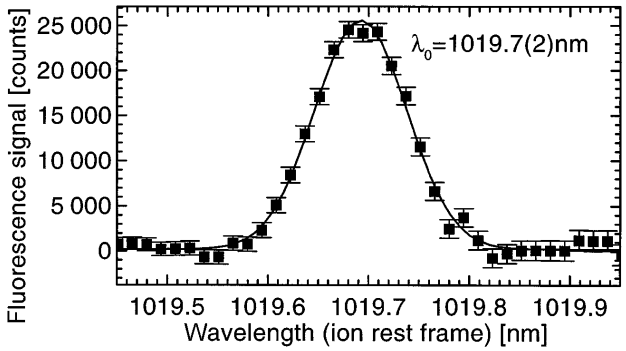

out more experiments with Ne, Ar and Kr HCI [59–61]. A novel transmission grating spectrometer with a very high efficiency and large optical aperture number was designed and built to improve resolution by Utter et al. [62]. With that instrument, they could improve the experimental accuracy of the measurements of the ground state fine structure of Ti-like ion in the cases of Pt^{56+}, Au^{57+}, and Tl^{59+} ions [63].

4. Hyperfine structure of H-like ions

The most extreme example of visible lines in HCI is the hyperfine transition in the ground state of H-like ions having nuclei with nonzero magnetic moment. The hyperfine structure of the ground state consists of only two levels, and the transition energy scales with the third power of Z. Thus, magnification of the splitting from the beginning of the periodic table to its end by a factor of nearly one million occurs, bringing the well-known microwave transition at 21 cm in atomic hydrogen well into the visible range at $Z > 60$. These lines are beautiful examples of a truly fundamental system: two bound charged particles in the highest stationary electromagnetic fields found in nature. The experimental difficulties to observe them were formidable, starting from the ion production and storage to the excitation and detection of a forbidden M1 transition. At the GSI in Germany, an adequate high-energy accelerator was able to bring bismuth ions to relativistic velocities, strip most of their electrons by shooting them through a thin foil, and inject the resulting H-like ions into a storage ring (ESR) of more than 100 m circumference. In a straight section of the machine, the circulating relativistic ions were excited by a collinear laser beam. Its wavelength was tuned to take the large Doppler shift into account. In 1994, the GSI laser spectroscopy group accomplished a fascinating experiment by Klaft et al. [64] to excite resonantly the H-like $^{209}Bi^{82+}$ ions from the ground state $1s\,^1S_{1/2}$, $F = 4$ into the first excited hyperfine state $1s\,^1S_{1/2}$, $F = 5$ at 243.87(4) nm and detect the subsequent fluorescence. Unfortunately, the maximum possible gain in accuracy was thwarted by the limited momentum resolution of the stored ion beam, which induces a large Doppler width, and by uncertainty in its

Fig. 9. Spectrum of the hyperfine transition $1s\ ^1S_{1/2}$, $F = 4 \rightarrow 3$ in $^{165}Ho^{66+}$ at 572.64(15) nm measured with the LLNL SuperEBIT [66] with an electron beam of 285 mA at 132 keV. Black/red curves: trap with/without Ho^{66+}.

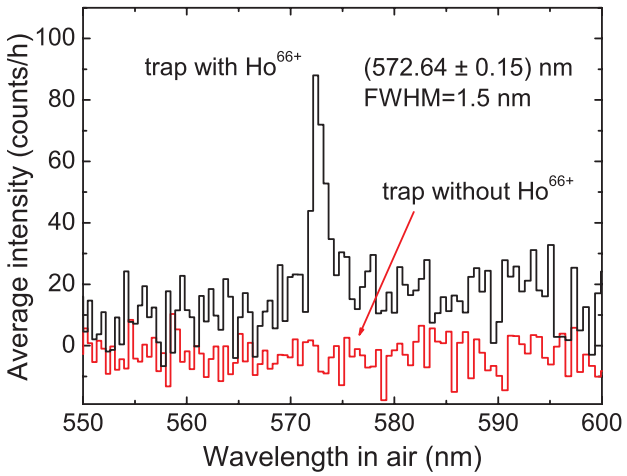

velocity, which causes a systematic error larger than the experimental line width. A resonance with a FWHM of 40 GHz was recorded, and the total uncertainty was 160 ppm. The same method was applied in 1998 to $^{207}Pb^{81+}$ by Seelig [65], who obtained 1019.7(2) nm (see Fig. 8) for the hyperfine ground-state transition in that ion. A disagreement of 4.5 nm compared to predictions was found, in spite of the apparent reliability of the nuclear size effect calculations used for the prediction of these essential contributions.

In the year 1995, the analogous $1s\ ^1S_{1/2}$, $F = 4 \rightarrow 3$ transition in $^{165}Ho^{66+}$ was detected using ions trapped in SuperEBIT [66], and its wavelength determined to be 572.64(15) nm (Fig. 9). Later, the ground-state hyperfine transitions were also measured for the H-like ions of two isotopes of rhenium, $^{185,187}Rh^{74+}$ with the same prism spectrograph [67] to be 456.05(30) and 451.69(30) nm, respectively. Two isotopes of thallium were investigated by means of a transmission grating spectrometer specifically developed for that purpose, described in ref. 62. The wavelengths for $^{203,205}Tl^{80+}$ were determined to be 385.822(30) and 382.184(34) nm, respectively [68]. The accuracy of the wavelength determination was in these cases limited by the statistics. This was a consequence of the small number of H-like ions (on the order of 10^5) trapped in the SuperEBIT, since radiative electron–ion recombination competes very strongly (with comparable or even larger cross section) with electron impact ionization at the electron beam energies attainable of less than 200 keV, and from the reduced light collection solid angle.

In the case of the Ho hyperfine splitting, an abnormally large deviation (8.9 nm) from the prediction was noticed. In view of the small estimated uncertainty for the QED contribution in those H-like ions, it was inferred that the nuclear parameters fed into the calculation had to be reviewed. Similar, if not so large, departures from predictions were found in all these hyperfine structure measurements from GSI and LLNL. The reason for these discrepancies results basically from the unreliability of the existing calculations of the Bohr–Weisskopf effect, i.e., the contribution of the nuclear magnetization distribution to the hyperfine splitting. After having taken into account relativistic, nuclear charge distribution, Bohr–Weisskopf and estimated QED corrections of approximately 54%, 4.5%, 1%, and 0.5% of the measured wavelength, respectively, the measured splitting was used in ^{165}Ho to determine the dipole magnetic momentum of the nucleus instead. The outcome confirmed the results of a more accurate independent measurement of that nuclear magnetic moment by the atomic beam resonance method (which had not been used for the initial prediction). Again, by using that independent value for the prediction of the splitting, the hyperfine measurement was consistent with the magnitude of the different theoretical contributions.

Following the same approach, namely, by using well-known nuclear magnetic moments and suitable corrections for the nuclear charge distribution and QED effects, the measured hyperfine splittings could be utilized to determine the mean square radii of the nuclear magnetization distribution. This application of reliable experimental values in combination with the predictions of the comparatively well-established QED theory of H-like ions to determine nuclear size parameters (which were previously loaded with much larger uncertainties) was not universally accepted in the beginning, but its merits have become clearer with time.

This issue remains one of the open problems for nuclear structure theory. As Beiersdorfer recently pointed out [69]:

> From the values we infer that models based on unpaired nucleons to determine the nuclear magnetization cannot accurately describe the observations.

Furthermore Beiersdorfer emphasizes:

> Unfortunately, calculations based on potentially more sophisticated models produce similar discrepancies, though with less clear or no systematics and thus provide less insight into the underlying physics than [those] calculations.

Gustavsson and Mårtensson-Pendrill [70] had also estimated in their theoretical study of these hyperfine transitions uncertainties of the order of 10^{-4} in the magnetic-shielding factor, or diamagnetic correction, caused by the bound electrons in the neutral atoms used for experimental determinations of the nuclear magnetic moment. Given the full electronic complexity of neutrals, full relativistic and QED atomic structure calculations are needed to predict the reduction of the effective magnetic field experienced by a nucleus immersed in an external field. This problem is also compounded with that of the chemical shift in cases where nuclear magnetic resonance methods are applied in the solid or liquid phase.

Addressing this issue from another point of view, Shabaev noted in ref. 71 that in contrast to the nonrelativistic case, where the corresponding correction is completely defined by the root-mean-square nuclear radius $\sqrt{\langle r^2 \rangle}$, in heavy ions the higher order moments of the nuclear charge distribution may affect the nuclear-size correction on a 1% accuracy level. Scaling these contributions from H-like to Li-like (i.e., basically, from $n = 1$ to 2) has been proposed by Shabaev to eliminate nuclear size contributions in first order. In view of these facts, one might

Fig. 10. Top view of the spectroscopic setup at the Freiburg (and later Heidelberg) EBIT, in which the electron beam flows horizontally. The horizontal image of the ion cloud is rotated and imaged 1:1 onto the entrance slit of the grating spectrometer ($f = 0.67$ m, grating with up to 3600 lines/mm, cryogenically cooled charge-coupled device detector).

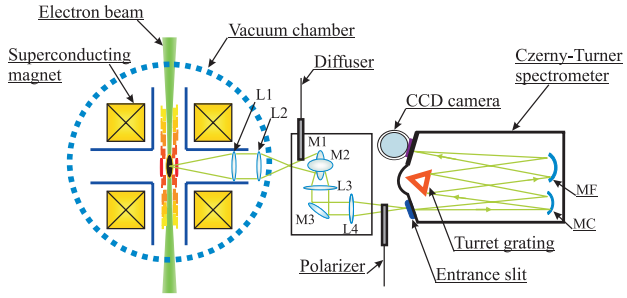

arrive at the conclusion that many of the decimal figures tabulated for the nuclear magnetic dipole moments are far less accurate than widely believed, as a consequence of the diamagnetic shielding and chemical shifts. The resulting uncertainties can add to roughly 0.1% of the total expected HFS splitting in HCI in some extreme cases. Therefore, systematic work aimed at understanding the exact magnitude of the diamagnetic shielding will be an essential task for HCI spectroscopy, with a particular emphasis in urgently needed hyperfine measurements in simple systems.

In summary, even the most basic data needed to analyze the hyperfine spectra, namely, the nuclear magnetic moment, appear to have problematic aspects when obtained by the study of neutral atoms, be they isolated or embedded in a solid. In future, HCI will provide a direct way of testing such diamagnetic effects by either spectroscopic methods or by nuclear resonance studies with HCI in Penning traps, where the magnetic g_J factor has been determined for low-Z H-like ions up to O^{6+} with the utmost accuracy [72].

The study of the nuclear structure using optical or laser spectroscopy in neutral atoms is a well established field. Starting from the discovery of the hyperfine structure, and thus of nuclear spin, of the hyperfine anomalies, nuclear deformations, and so on, extremely valuable data have been harvested by atomic spectroscopy methods. But the combination of optical spectroscopy and HCI offers new avenues for this type of work. The essential advantages are derived firstly from the simplification of the electronic structure intrinsic to a HCI, and secondly from the $\propto Z^4$ (Z: atomic number, and by extension ionic charge state) and $\propto 1/n^3$ (n: principal quantum number) scaling laws governing the magnitude of nuclear contributions to the electronic binding energy. Furthermore, here, nearly undisturbed nuclei are tested with the most natural probe, the deeply bound electrons surrounding them. In such a stable, long-lived quantum system, the electronic wave function interrogates the nuclear charge and magnetization distributions continuously and "adjusts" the binding energy by amounts corresponding to 10% and nearly 2% of the total transition energy for the ground state hyperfine transition in the heavy H-like ions, respectively. While these effects might appear to become too small for the shells with higher principal quantum numbers $n = 2, 3, 4,$

Fig. 11. Spectrum of the Ar^{13+} $1s^2\,2s^2\,2p\,^2P_{3/2} \rightarrow {}^2P_{1/2}$ transition at 441.256 nm at the Heidelberg EBIT. By increasing the neutral gas density in the trap by means of a dense atomic beam, calibration lines from neutral and singly charged Ar ions (marked with red solid circles) are excited in nearly the same volume where the HCI are trapped.

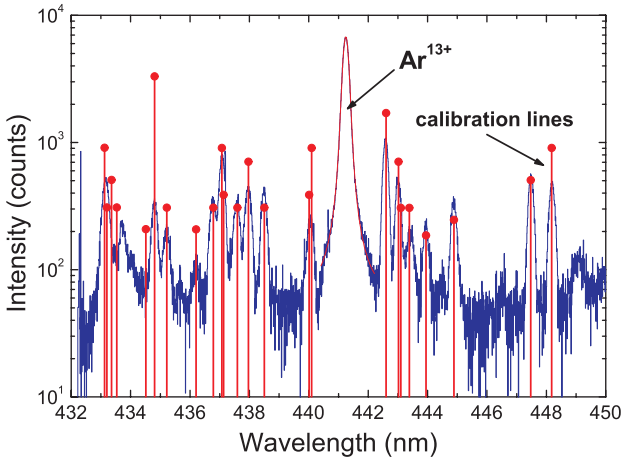

the excellent accuracy of optical (or better, laser) spectroscopic methods, and the fact that the large variety of transitions available offer different levels of sensitivity to the finite nuclear size and QED contributions are compelling arguments for their systematic investigation.

5. QED contributions to the binding energy

The accuracy of EBIT measurements in the visible range has improved steadily over time. At the EBIT developed at the Freiburg University in 1999 [73], which was transferred to the Max Planck Institute for Nuclear Physics in Heidelberg in the year 2001, a Czerny–Turner grating spectrometer with 0.67 m focal length and cryogenic CCD was set up (Fig. 10). A set of lenses built inside the EBIT vacuum chamber improved the optical collection efficiency. Calibration techniques had also been improved in the meantime. Several methods were applied simultaneously (as noted in refs. 74 and 76) to cross check the calibrations against each other. In one of them, the lines emitted by neutrals and low-charge ions are intentionally boosted by increasing the injection pressure on the expansion stage of the differentially pumped atomic beam used at the EBIT. Such a spectrum is displayed in Fig. 11.

This method was found equally reliable as the use of external calibration lamps, albeit more cumbersome, for the EBIT operation. Hollow-cathode discharge lamps provided lines much narrower than those from standard low-pressure pencil-type lamps, and were also nearly unaffected by plasma broadening and Stark shifts. By using many lines to calibrate a nearly linearly dispersive spectrometer, it was finally possible to reach an accuracy in the sub-ppm range.

Draganič [74] dedicated careful studies to the four- and five-electron ions, and in particular to those of Ar. Their wavelengths were found for the B-like $^2P_{3/2} \rightarrow {}^2P_{1/2}$ transition in Ar^{13+} to be 441.2559(1) nm and for the Be-like $^3P_2 \rightarrow {}^3P_1$ transition in

Table 1. Comparison of the wavelength predicted for the $1s^2\,2s\,2p\,{}^3\mathrm{P}_2 \rightarrow {}^3\mathrm{P}_1$ transition in Be-like Ar^{14+} by configuration interaction (CI) Dirac–Fock methods including quantum electrodynamic (QED) contributions and the experimental results of Draganič [74].

Dirac–Fock with CI	596.1100 ± 0.1100
QED contributions	-1.8900 ± 0.2800
Total theory	594.2200 ± 0.3000
Experiment	$\mathbf{594.3880 \pm 0.0003}$

Fig. 12. Four spectra of the Ar^{13+} $1s^2\,2s^2\,2p\,{}^2\mathrm{P}_{3/2} \rightarrow {}^2\mathrm{P}_{1/2}$ transition at 441.256 nm showing growing resolution as the ion temperature was lowered. Evaporative cooling was enhanced (from the top to the bottom spectrum) by decreasing the trapping potential both axially (by lowering the voltages applied to the drift tubes) and radially (by decreasing the electron beam current).

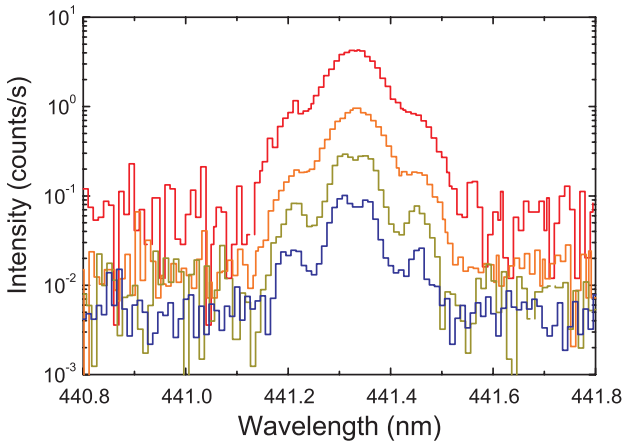

Ar^{14+} to be 594.3880(5) nm, respectively. In both cases, QED contributions to the transition energy are about 6000 larger than experimental uncertainty, which had been reduced to 0.3 ppm. In the earlier calculations included in ref. 74, the uncertainty of the terms obtained by the configuration interaction Dirac–Fock method was smaller than that of the QED part of the prediction, as shown in Table 1. Thus, a limited test of the QED corrections was already possible. The broad spectral features of the HCI were still problematic. To further enhance the wavelength accuracy, choosing a narrow slit was an obvious choice to reduce source broadening. Still, the Doppler width of the lines remained an issue. To counteract this, the technique of evaporative cooling was applied by Soria Orts [75] to lower the translational temperature T_{ion} of the trapped ions from values typically found at EBITs of several hundred eV down to only $T_{\mathrm{ion}} \approx 6$ eV, the lowest temperature reported in such a trap.

This was accomplished by intentionally reducing both the axial trapping voltage (essentially to zero) and the electron beam current (down to a few mA) , resulting in enhanced evaporation of hot ions effectively cooling the remaining trapped ions (see Fig. 12). The corresponding intensity losses of two orders of magnitude could be tolerated due to the very good optical collection efficiency of the system. A considerable decrease in the spectral width of the emission lines resulted, and in fact even the Zeeman splitting of the lines of interest could be clearly observed, as displayed in Fig. 13. The two spectra displayed in Fig. 13 were recorded by using a polarization filter in two different orientations, parallel and perpendicular to the magnetic field. The σ and π components of M1 transitions show a characteristic alignment to the magnetic field just opposite to that of the E1 transitions. In this setup, the field-dependent Zeeman splitting was measured at various field strengths, and Landé factors g_J could be determined. Good agreement with theory was found, but no significant test of the predictions could be made at the attained resolution [77].

Fig. 13. The Zeeman components of the Ar^{13+} $1s^2\,2s^2\,2p^1\,{}^2\mathrm{P}_{3/2} \rightarrow {}^2\mathrm{P}_{1/2}$ transition at 441.256 nm observed transversally to a magnetic field of 6.82 T (20 mA beam current, 850 eV beam energy). Note that σ and π components of M1 transitions display an opposite polarization behavior as in the E1 transition lines. The ion translational temperature was estimated to be $T_{\mathrm{ion}} = 6$ eV after deconvolving the apparatus profile of the grating spectrometer used (from Soria Orts [75–77]).

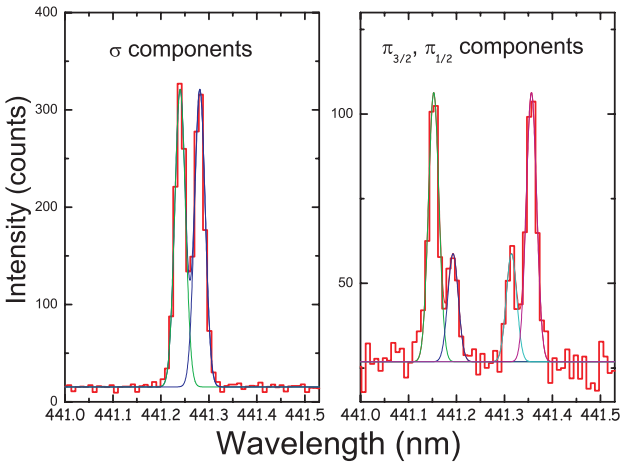

A recent example of an application of precisely these Ar^{q+} forbidden lines to the diagnostics of the inner and outer edge plasma in a magnetic fusion device, the Large Helical Device can be found in the work of Iwamae et al. [78]. Spectra like those shown in Fig. 14 were recorded, in which the Zeeman splitting was also used as a diagnostic of the local magnetic fields.

6. Isotopic shifts

In the recent paper of Soria Orts [76], the effects of the relativistic nuclear recoil were investigated in a very convenient system, namely, ^{40}Ar:^{36}Ar. The isotopic shifts of the forbidden lines $1s^2\,2s^2\,2p\,{}^2\mathrm{P}_{3/2} \rightarrow {}^2\mathrm{P}_{1/2}$ in Ar^{13+} and $1s^2\,2s\,2p\,{}^3\mathrm{P}_2 \rightarrow {}^3\mathrm{P}_1$ in Ar^{14+} were measured with high precision. For that purpose, an atomic beam either from ^{40}Ar or ^{36}Ar was injected into the trap. By extracting ions from the trap and measuring their q/m (charge/mass) ratios, the isotopic composition was tested. Wavelength calibration was carried out with an iron hollow-cathode lamp. About ten lines contained over a range of

Fig. 14. Line profiles of E1 transitions of Ar II and the M1 transition Ar^{13+} $1s^2\,2s^2\,2p^1\,{}^2P_{3/2} \rightarrow {}^2P_{1/2}$ transition at 441.256 nm. Spectra for two polarization components obtained at the Large Helical Device by Iwamae [78]. Polarized light was registered in 166° and 76° directions approximately parallel and perpendicular to the magnetic field direction, respectively. The figure from ref. 78. Reprinted with permission from the American Institute of Physics. © 2007, American Institute of Physics.

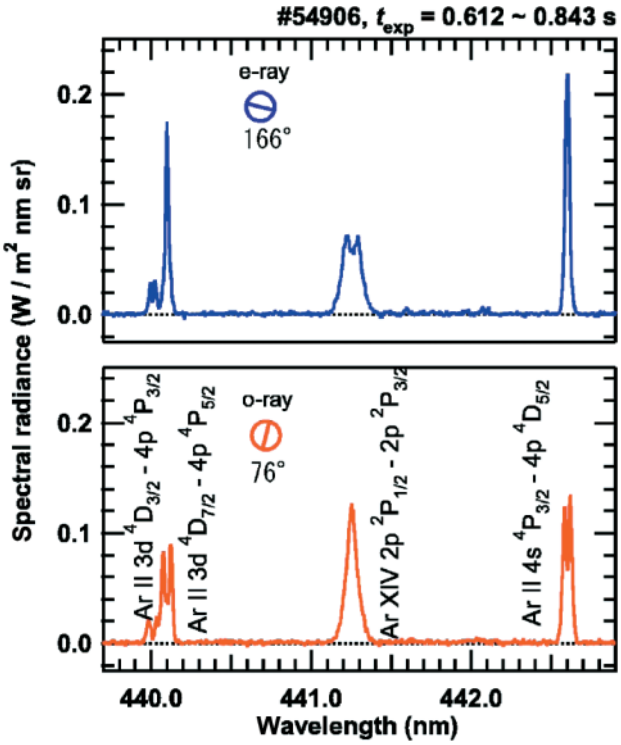

15 nm with interferometrically established wavelengths were recorded in each calibration spectrum. Their values were then plotted versus their centroid pixel positions, and the resulting curve, which deviates only very weakly from a straight line, was fitted to a parabola to obtain the instrument dispersion curve. Individual calibrations were carried out before and after each measurement of the argon lines to reduce the effect of possible long-term shifts of the setup. The calibration lines displayed a FWHM of only a few pixels. To avoid sampling errors of their individual line profiles and to minimize statistical uncertainty, 15–30 spectra of 30–50 min each were recorded for every line together with their corresponding calibration spectra, while gradually shifting the grating by a small angle between measurements. In this way, each CCD pixel could be viewed as an exit slit sampling the line profile in very small angular steps of the grating rotation, thus avoiding sampling errors. The laboratory was temperature stabilized. By these means, the very small isotopic shift could be accurately determined. The experimental results of Soria Orts [76] are compared with predictions including those various contributions in Table 2. Good agreement with the experimental data for both the Ar^{13+}, and the Ar^{14+} forbidden lines confirms the results of these calculations.

The 10% change of the nuclear mass induces only a minute wavelength difference of around 0.0012 nm. For this ion with a relatively low-Z value ($Z = 18$), the shift is not caused by the nuclear finite size effect (FS) but is due to relativistic kinematic effects that cannot be accounted for within the well-known reduced mass treatment of the nuclear recoil problem in neutral atoms, the so-called normal mass shift (NMS). The optical electron, of the $Ar^{13+,14+}$ ions, in contrast to those of neutrals, is bound by 700 and 856 eV, and, therefore, exerts a pull on the nucleus with already noticeable relativistic contributions. These corrections had not been treated theoretically in a consistent way until recently. In 1985, Shabaev [79] found a rigorous solution of the problem, and established that earlier predictions on this subject had been nearly meaningless, in particular, those regarding the specific mass shift (SMS), or relativistic mass polarization term. These contributions are induced by the correlated motion of all bound electrons. Palmer also derived independently a reformulation of the theory of the mass shift [80], obtaining essentially the same Hamiltonian, and pointing out to the theoretical inconsistencies which appear when the NMS term is used in relativistic problems.

Table 2. Nonrelativistic, relativistic, and QED contributions (given in cm^{-1}) to the $^{40}Ar/^{36}Ar$ mass isotope shift for the forbidden lines of Ar^{13+} at 441.256 nm and Ar^{14+} at 594.388 nm, and predicted total isotopic shifts compared with experimental results (given in nm) [76]. NMS: normal mass shift; RNMS: relativistic corrections to NMS; SMS: specific mass shift (or mass polarization term); RSMS: relativistic corrections to SMS; FS: finite size (nuclear) corrections.

	Ar^{13+}	Ar^{14+}
NMS	0.105 245	0.079 615
RNMS	−0.082 153	−0.062 695
One-electron QED	0.000 177	0.000 187
SMS	−0.074 135	−0.069 737
RSMS	0.115 136	0.088 714
Two-electron QED	−0.000 799	−0.001 527
FS	−0.000 514	−0.000 120
Sum	**0.062 957**	**0.034 437**
Isotope shift (nm):		
Theory	0.001 23(5)	0.001 22(5)
Experiment	**0.001 23(6)**	**0.001 20(10)**

7. New theoretical developments

Indelicato [81] and Doron [82] have studied theoretically the Zr-like isoelectronic sequence, which has a $4d^4$ ground-state configuration. Forbidden transitions with a Z dependence similar to that of the Ti-like sequence are predicted there. However, the calculations have estimated relative uncertainties in wavelength as large as 10%. The intensity ratios of these lines are expected to provide useful tools for plasma diagnostics at electron densities in the range $n_e \approx 10^9$ to 10^{14} cm^{-3}. From another point of view, these electronic transitions involve a bound electron with a large relativistic energy component in the $n = 4$ shell. This could also become an interesting method of testing the sensitivity of their wave functions to nuclear size parameters scaling with $1/n^3$.

From the point of view of fundamental QED studies, good theoretical progress has been achieved in the last years. In very recent ab initio QED calculations for the B-like Ar^{13+} ion, Artemyev et al. [83] introduced a screening potential (for which they tested four different models) into the usual QED perturbation calculations using the Furry picture, thus adding a dominant part of the interelectronic interaction to the zero-order Hamiltonian. The two-time Green function method developed by Shabaev [84] was applied. By using a special representation of the Hamiltonian separating the electron–electron (Coulomb and Breit) and electron–nucleus interactions it becomes possible to expand the energy term in a powers series. The expansion coefficients correspond to the first- and second-order QED interaction diagrams in the Breit approximation. Contributions adding up to 49 cm^{-1} and 2 cm^{-1}, respectively, were determined for those QED terms. The predictions include rigorous QED calculations for the two lowest order QED and electron-correlation terms. Third-order and higher order electron-correlation contributions were approximated by the configuration interaction Dirac–Fock method. The agreement of the predicted value of 441.261(70) nm (given in air) with the result of Draganič [74] of 441.2559(1) nm, (also given in air) is excellent. These calculations represent a significant advance in the understanding of the interplay of electron–electron QED interaction and screening in the presence of extremely high nuclear electromagnetic fields.

8. Summary and outlook at open challenges

Observations of the visible spectrum from HCI have been essential for the discovery and understanding of astrophysical plasmas and still play an important role not only there, but also for the diagnostics of high-temperature plasmas and for the study of fundamental interactions, in particular of QED in high fields. EBITs have evolved into excellent tools for these investigations, producing ions of the desired charge states under well-defined conditions. The accuracy of experimental HCI spectral data in this range surpasses that in any other region. Initial measurements in the Ti-like isoelectronic sequence showed an unexpected disagreement with predictions, clearly pointing at more general underlying problems of few-electron relativistic structure theory. Recent state-of-the-art, rigorous many-electron QED calculations have somewhat narrowed the lead in accuracy by the benchmark experiments. Isotopic shifts of forbidden transitions in HCI have confirmed the currently most sophisticated treatment of the relativistic nuclear recoil. Data on the hyperfine structure of H-like ions have shown that nuclear size effects are not yet reliably predicted by theory. Dedicated studies of such effects with HCI along several isoelectronic sequences to extract the genuine QED part will be a prerequisite for a systematic test of the nonperturbative theory of QED in strong electromagnetic fields. In the near future, work with HCI in the optical range will continue in several laboratories worldwide. Hyperfine quenching experiments are planned at the Shanghai EBIT [85]. Nuclear-size-effect studies with radioactive ions will become possible at several facilities, like TITAN at TRIUMF, the NSCC laboratory at MSU, and HITRAP at GSI. With the availability of a wider variety of isotopes for EBIT experiments, the mutual interplay of nuclear size effects and QED contributions may well be disentangled satisfactorily by means of systematic studies along isotopic chains. Parity violation experiments with them might eventually also become feasible. Novel ion cooling schemes have been proposed for trapped HCI to improve the resolution. Ultimately, the current work in progress on experiments applying laser spectroscopic techniques to the forbidden lines of HCI in EBITs and other traps, and in particular to the hyperfine transitions of H-like ions that have already been investigated in such devices by the techniques described above may result in extremely stable frequency standards.

Acknowledgments

The author wants to express his gratitude to all the people involved in the experiments reviewed here, and in particular to his former coworkers Ilija Draganič and Rosario Soria Orts, who carried out the laboratory work in Freiburg and Heidelberg, to Joachim Ullrich, as well as to Peter Beiersdorfer, Steven Utter and Klaus Widmann from LLNL, and to Elmar Träbert. Thanks also to Anne-Marie Mårtensson-Pendrill, Martin Gustavsson, Ilya Tupitsyn, Anton Artemyev, Vladimir Shabaev, Ulrich Jentschura, Christoph Keitel, and Zoltan Harman, who have accompanied many of these experiments as theoreticians. Part of this work was performed under the auspices of the U.S. DOE by the University of California Lawrence Livermore National Laboratory under contract W-7405-ENG-48. Work in Freiburg and Heidelberg was supported by the Deutsche Hochschulbauförderung, the University of Freiburg, the Deutsche Forschungsgemeinschaft (Leibniz Programm and contract ULL 166/2-1), and the Max Planck Institute for Nuclear Physics.

References

1. C.A. Young. The Sun and the phenomena of its atmosphere. C.C. Chatfield & Co., New Haven, Connecticut. 1872.
2. W. Grotrian. Zeit. Astrophys. **7**, 26 (1933).
3. W. Grotrian. Naturwissenschaften, **27**, 214 (1939).
4. B. Edlén. Z. Astrophys. **22**, 30 (1943).
5. B. Lyot. Comptes Rendues Acad. Sci. **202**, 1259 (1936).
6. H. Alfvén. Arkiv för Matem. Astron. och Fysik, **27A**, 25 (1941).
7. M. Fischer, N. Kolachevsky, M. Zimmermann, R. Holzwarth, Th. Udem, T.W. Hänsch, M. Abgrall, J. Grünert, I. Maksimovic, S. Bize, H. Marion, F. Pereira Dos Santos, P. Lemonde, G. Santarelli, P. Laurent, A. Clairon, C. Salomon, M. Haas, U.D. Jentschura, and C.H. Keitel. Phys. Rev. Lett. **92**, 230802 (2004).
8. J.K. Webb, M.T. Murphy, V.V. Flambaum, V.A. Dzuba, J.D. Barrow, C.W. Churchill, J.X. Prochaska, and A.M. Wolfe. Phys. Rev. Lett. **87**, 091301 (2001).
9. R. Srianand, H. Chand, P. Petitjean, and B. Aracil. Phys. Rev. Lett. **92**, 121302 (2004).
10. P. Swings. Astrophys. J. **98**, 119 (1943).
11. W.J. Wagner and L.L. House. Sol. Phys. **54**, 55 (1968).
12. J.H.M.M. Schmitt and R. Wichmann. Nature, **412**, 508 (2001).
13. S. Suckewer and E. Hinnov. Phys. Rev. Lett. **41**, 756 (1978).

14. E. Hinnov. Nucl. Instrum. Methods, **202**, 381 (1982).
15. S.I. Lippman, K.B. Fournier, A.L. Osterheld, and W.H. Goldstein. Phys. Rev. E, **51**, 5139 (1995).
16. M.H. Prior. J. Opt. Soc. Am. B, **4**, 144 (1987).
17. M.A. Levine, R.E. Marrs, J.R. Henderson, D.A. Knapp, and M.B. Schneider. Phys. Scr. **T22**, 157 (1988).
18. M.A. Levine, R.E. Marrs, J.N. Bardsley, P. Beiersdorfer, C.L. Bennett, M.H. Chen, T. Cowan, D. Dietrich, J.R. Henderson, D.A. Knapp, A. Osterheld, B.M. Penetrante, M.B. Schneider, and J.H. Scofield. Nucl. Instrum. Methods Phys. Res. B, **43**, 431 (1989).
19. R.E. Marrs, P. Beiersdorfer, and D. Schneider. Phys. Today, **47**, 27 (1994).
20. U. Feldman, P. Indelicato, and J. Sugar. J. Opt. Soc. Am. B, **8**, 3 (1991).
21. C.A. Morgan, F.G. Serpa, E. Takács, E.S. Meyer, J. Sugar, J.R. Roberts, C.M. Brown, and U. Feldman. Phys. Rev. Lett. **74**, 1716 (1995).
22. J.D. Gillaspy, Y. Aglitskiy, E.W. Bell, C.M. Brown, C.T. Chantler, R.D. Deslattes, U. Feldman, L.T. Hudson, J.M. Laming, E.S. Meyer, C.A. Morgan, A.I. Pikin, J.R. Roberts, L.P. Ratliff, F.G. Serpa, J. Sugar, and E. Takács. Phys. Scr. **T59**, 392 (1995).
23. H. Adler, E.S. Meyer, F.G. Serpa, E. Takács, J.D. Gillaspy, C.M. Brown, and U. Feldman. Nucl. Instrum. Methods Phys. Res. B, **98** 581 (1995).
24. R.D. Cowan. The theory of atomic structure and spectra. University California Press, Berkeley, Calif. 1981.
25. F.G. Serpa, E.S. Meyer, C.A. Morgan, J.D. Gillaspy, J. Sugar, J.R. Roberts, C.M. Brown, and U. Feldman. Phys. Rev. A, **53**, 2220 (1996).
26. F.G. Serpa, E.W. Bell, E.S. Meyer, J.D. Gillaspy, and J.R. Roberts. Phys. Rev. A, **55**, 1832 (1997).
27. P. Beiersdorfer, L. Schweikhard, J.R. Crespo López-Urrutia, and K. Widmann. Rev. Sci. Instrum. **67**, 3818 (1996).
28. F.G. Serpa, C.A. Morgan, E.S. Meyer, J.D. Gillaspy, E. Träbert, D.A. Church, and E. Takaćs. Phys. Rev. A, **55**, 4196 (1997).
29. F.G. Serpa, J.D. Gillaspy, and E. Träbert. J. Phys. B: At. Mol. Opt. Phys. **31**, 3345 (1998).
30. J.D. Gillaspy. J. Phys. B: At. Mol. Opt. Phys. **34**, R93 (2001).
31. E. Träbert, P. Beiersdorfer, S.B. Utter, and J.R. Crespo Lopez-Urrutia. Phys. Scr. **58**, 599 (1998).
32. E. Träbert. Can. J. Phys. **80**, 1481 (2002).
33. E. Träbert, P. Beiersdorfer, G. Gwinner, E.H. Pinnington, and A. Wolf. Phys. Rev. A, **66**, 052507 (2002).
34. P. Beiersdorfer, E. Träbert, and E.H. Pinnington. Astrophys. J. **587**, 836 (2003).
35. A. Lapierre, U.D. Jentschura, J.R. Crespo López-Urrutia, J. Braun, G. Brenner, H. Bruhns, D. Fischer, A.J. González Martínez, Z. Harman, W.R. Johnson, C.H. Keitel, V. Mironov, C.J. Osborne, G. Sikler, R. Soria Orts, V.M. Shabaev, H. Tawara, I.I. Tupitsyn, J. Ullrich, and A. Volotka. Phys. Rev. Lett. **95**, 183001 (2005).
36. A. Lapierre, J.R. Crespo López-Urrutia, J. Braun, G. Brenner, H. Bruhns, D. Fischer, A.J. González Martínez, V. Mironov, C. Osborne, G. Sikler, R. Soria Orts, H. Tawara, and J. Ullrich. Phys. Rev. A, **73**, 052507 (2006).
37. G. Brenner, J.R. Crespo López-Urrutia, Z. Harman, P.H. Mokler, and J. Ullrich. Phys. Rev. A, **75**, 032504 (2007).
38. F.J. Currell, J. Asada, K. Ishii, A. Minoh, K. Motohashi, N. Nakamura, K. Nishizawa, S. Ohtani, K. Okazaki, M. Sakurai, H. Shiraishi, S. Tsurubuchi, and H. Watanabe. J. Phys. Soc. Jpn. **65**, 3186 (1996).
39. F.J. Currell, D. Kato, N. Nakamura, S. Ohtani, E.J. Sokell, H. Watanabe, and C. Yamada. Phys. Scr. **T80**, 154 (1999).
40. H. Watanabe, D. Kato, T. Kinugawa, S. Ohtani, and C. Yamada. Phys. Scr. **T92**, 122 (2001).
41. H. Watanabe, D. Crosby, F.J. Currell, T. Fukami, D. Kato, S. Ohtani, J.D. Silver, and C. Yamada. Phys. Rev. A, **62**, 042513 (2001).
42. H. Kuramoto, I. Yamada, T. Kinugawa, C. Yamada, and S. Ohtani. Beam diagnostics by Thomson scattering with the Tokyo-EBIT, 10th International Conference on the Physics of Highly Charged Ions, Univ. of California-Berkeley, USA. July 2000; also in H. Kuramoto, I. Yamada, H. Watanabe, M. Sawasaki, C. Yamada, and S. Ohtani. Phys. Scr. **T92**, 351 (2001).
43. G.J. Herrmann. J. Appl. Phys. **29**, 127 (1958).
44. J.V. Porto, I. Kink, and J.D. Gillaspy. Rev. Sci. Instrum. **71**, 3052 (2000).
45. J.V. Porto, I. Kink, and J.D. Gillaspy. Phys. Rev. A, **61**, 054501 (2000).
46. E. Takács, B. Blagojevic, K. Makónyi, E.-O. Le Bigot, C.I. Szabó, Y.-K. Kim, and J.D. Gillaspy. Phys. Rev. A, **73**, 052505 (2006).
47. C. Biedermann and R. Radtke, Phys. Rev. A 75, 066501 (2007)
48. J.R. Crespo López-Urrutia, P. Beiersdorfer, and K. Widmann. 19th International Conference on the Physics of Electronic and Atomic Collisions ICPEAC. 26th July–1st August 1995. Whistler, BC, Canada. Book of abstracts. Vol. 2, p. 589.
49. J.R. Crespo López-Urrutia, P. Beiersdorfer, K. Widmann, and V. Decaux. Phys. Scr. **T80**, 448 (1999).
50. J.R. Crespo López-Urrutia, P. Beiersdorfer, K. Widman, and V. Decaux. Can. J. Phys. **80**, 1687 (2002).
51. J.D. Silver, A.J. Varney, H.S. Margolis, P.E.G. Baird, I.P. Grant, P.D. Groves, W.A. Hallett, A.T. Handford, P.J. Hirst, A.R. Holmes, D.J.H. Howie, R.A. Hunt, K.A. Nobbs, M. Roberts, W. Studholme, J.S. Wark, M.T. Williams, M.A. Levine, D.D. Dietrich, W.G. Graham, I.D. Williams, R. O'Neil, and S.J. Rose. Rev. Sci. Instrum. **65**, 1072 (1994).
52. D.J. Bieber. DPhil. thesis, University of Oxford. 1997.
53. D.J. Bieber, H.S. Margolis, P.K. Oxley, and J.D. Silver. Phys. Scr. **T73**, 64 (1997).
54. D.N. Crosby, K. Gaarde-Widdowson, J.D. Silver, and M.R. Tarbutt. Phys. Scr. **T92**, 144 (2001).
55. H.S. Margolis, P.D. Groves, J.D. Silver, and M.A. Levine. Hyperfine Interact. **99**, 169 (1996).
56. T.V. Back, P.D. Groves, H.S. Margolis, P.K. Oxley, and J.D. Silver. Phys. Scr. **T73**, 62 (1997).
57. T.V. Back, H.S. Margolis, P.K. Oxley, J.D. Silver, and E.G. Myers. Hyperfine Interact. **114**, 203 (1998).
58. H. Chen, P. Beiersdorfer, C.L. Harris, S.B. Utter, and K.L. Wong. Rev. Sci. Instrum. **72**, 983 (2001).
59. H. Chen, P. Beiersdorfer, C.L. Harris, E. Träbert, S.B. Utter, and K.L. Wong. Phys. Scr. **T92**, 284 (2001).
60. H. Chen, P. Beiersdorfer, C.L. Harris, and S.B. Utter. Phys. Scr. **65**, 252 (2002).
61. H. Chen, P. Beiersdorfer, C.L. Harris, and S.B. Utter. Phys. Scr. **66**, 133 (2002).

62. S.B. Utter, J.R. Crespo López-Urrutia, P. Beiersdorfer, and E. Träbert. Rev. Sci. Instrum. **73**, 3737 (2002).
63. S.B. Utter, P. Beiersdorfer, and E. Träbert. Phys. Rev. A, **67**, 012508 (2003).
64. I. Klaft, S. Borneis, T. Engel, B. Fricke, R. Grieser, G. Huber, T. Kühl, D. Marx, R. Neumann, S. Schröder, P. Seelig, and L. Völker. Phys. Rev. Lett. **73**, 2425 (1994).
65. P. Seelig, S. Borneis, A. Dax, T. Engel, S. Faber, M. Gerlach, C. Holbrow, G. Huber, T. Kühl, D. Marx, K. Meier, P. Merz, W. Quint, F. Schmitt, M. Tomaselli, L. Völker, H. Winter, M. Würtz, K. Beckert, B. Franzke, F. Nolden, H. Reich, M. Steck, and T. Winkler. Phys. Rev. Lett. **81**, 4824 (1998).
66. J.R. Crespo López-Urrutia, P. Beiersdorfer, D. Savin, and K. Widman. Phys. Rev. Lett. **77**, 826 (1996).
67. J.R. Crespo López-Urrutia, P. Beiersdorfer, K. Widmann, A.-M. Mårtensson-Pendrill, and M.G.H. Gustavsson. Phys. Rev. A, **57**, 879 (1998).
68. P. Beiersdorfer, S.B. Utter, K.L. Wong, J.R. Crespo López-Urrutia, J.A. Britten, H. Chen, C.L. Harris, R.S. Thoe, D.B. Thorn, and E. Träbert. Phys. Rev. A, **64**, 032506 (2001).
69. P. Beiersdorfer. Phys. Scr. **T120**, 40 (2005).
70. M.G.H. Gustavsson and A.-M. Mårtensson-Pendrill. Phys. Rev. A, **58**, 3611 (1998).
71. V.M. Shabaev, A.N. Artemyev, V.A. Yerokhin, O.M. Zherebtsov, and G. Soff. Phys. Rev. Lett. **86** 3959 (2001).
72. J. Verdú, S. Djekić, S. Stahl, T. Valenzuela, M. Vogel, and G. Werth. Phys. Rev. Lett. **92**, 093002 (2004).
73. J.R. Crespo López-Urrutia, B. Bapat, B. Feuerstein, A. Werdich, and J. Ullrich. Hyperfine Interact. **127**, 497 (2000).
74. I. Draganič, J.R. Crespo López-Urrutia, R. DuBois, S. Fritzsche, V.M. Shabaev, R. Soria Orts, I.I. Tupitsyn, Y. Zou, and J. Ullrich. Phys. Rev. Lett. **91**, 183001 (2003).
75. R. Soria Orts. Isotopic effect in B-like and Be-like argon ions, Dissertation. University of Frankfurt. 2005; http://www.atom.uni-frankfurt.de/web/publications/files /RosarioSoria2005.pdf
76. R. Soria Orts, Z. Harman, J.R. Crespo López-Urrutia, A.N. Artemyev, H. Bruhns, A.J. González Martínez, U.D. Jentschura, C.H. Keitel, A. Lapierre, V. Mironov, V.M. Shabaev, H. Tawara, I.I. Tupitsyn, J. Ullrich, and A.V. Volotka. Phys. Rev. Lett. **97**, 103002 (2006).
77. R. Soria Orts, J.R. Crespo López-Urrutia, H. Bruhns, A.J. González Martínez, Z. Harman, U.D. Jentschura, C.H. Keitel, A. Lapierre, H. Tawara, I.I. Tupitsyn, J. Ullrich, and A.V. Volotka. Phys. Rev. A, **76**, 052501 (2007).
78. A. Iwamae, M. Atake, A. Sakaue, R. Katai, M. Goto, and S. Morita. Phys. Plasmas, **14**, 042504 (2007).
79. V.M. Shabaev. Teor. Mat. Fiz. **63**, 394 (1985) [Theor. Math. Phys. (Engl. Transl.) **63**, 588 (1985)]; Yad. Fiz. **47**, 107 (1988) [Sov. J. Nucl. Phys. **47**, 69 (1988).]
80. C.W. Palmer. J. Phys. B, **20**, 5987 (1987).
81. P. Indelicato. Phys. Scr. **T65**, 57 (1996).
82. R. Doron and U. Feldman. Phys. Scr. **64**, 219 (2001).
83. A.N. Artemyev, V.M. Shabaev, I.I. Tupitsyn, G. Plunien, and V.A. Yerokhin. Phys. Rev. Lett. **98**, 173004 (2007).
84. V.M. Shabaev. Phys. Rep. **356**, 119 (2002).
85. K. Yao, M. Andersson, T. Brage, R. Hutton, P. Jönsson, and Y. Zou. Phys. Rev. Lett. **97**, 183001 (2006).